Estimation of Global Leaf Area Index and Absorbed Par Using Radiative Transfer Models

Ranga B. Myneni, Ramakrishna R. Nemani, and Steven W. Running

***Abstract*— A simple method for the estimation of global leaf area index (LAI) and fraction of photosynthetically active radiation absorbed by the vegetation (FAPAR) from atmospherically corrected Normalized Difference Vegetation Index (NDVI) observations is described. Recent improvements to our three dimensional radiative transfer model of a vegetated surface are described. Example simulation results and a validation exercise are discussed. The model was utilized to derive land cover specific NDVI–LAI and NDVI–FAPAR relations. The method therefore requires stratification of global vegetation into cover types that are compatible with the radiative transfer model. Such a classification based on vegetation structure is proposed and a simple method for its derivation is presented. Proof-of-concept results are given to illustrate the feasibility of the proposed method.**

***Index Terms*— EOS, FPAR, LAI, MISR, MODIS, radiative transfer, remote sensing.**

I. Introduction

THE importance of vegetation in studies of global climate and biogeochemical cycles is now well recognized [1]. This is especially the case with respect to carbon, with about a quarter of atmospheric carbon dioxide potentially fixed as gross primary production by terrestrial vegetation annually [2]. In order to estimate carbon fixation by terrestrial vegetation and to prescribe the land surface accurately in global climate models, variables descriptive of surface assimilation area, radiation absorption, plant physiology and climatology are required. The general consensus is that such multitemporal global data sets can be regularly obtained only from remote sensing. Therefore, several of the instruments scheduled for the Earth Observing System (EOS) have land surface parameter estimation as major deliverables [3].

Two key variables required in primary production and global climate studies are leaf area index (LAI) and fraction of photosynthetically active radiation (0.4–0.7 μm) absorbed by the vegetation (FAPAR) [4], [5]. Leaf area index is generally defined as one-sided green leaf area per unit ground area in broadleaf canopies, and variously (projected or total) in needle canopies. Unlike LAI, FAPAR exhibits diurnal variation. Its use in models with time steps longer than a day requires appropriate time integration. The only global data set of LAI, FAPAR and other important surface variables available at the present time is the so-called FASIR (Fourier Adjusted, Solar zenith angle corrected, Interpolated and Reconstructed) data set [6], [7]. It is a $1.0^\circ \times 1.0^\circ$ monthly data set based on nine years of Advanced Very High Resolution Radiometer (AVHRR) data, with Fourier adjustment for smoothing, data reconstruction in the northern high latitudes, and sun-angle corrections. The FASIR algorithm is described in [6] and [7]; it suffices here to note that the algorithm is not based on physical principles of remote sensing (i.e., radiative transfer in vegetation and atmosphere) but on heuristic corrective methods to obtain spatially continuous multiyear data sets of surface variables, primarily for use in global climate models. A semi-physical algorithm for the estimation of LAI was reported by Price [8]. This algorithm requires certain constants to be estimated from the image data and it is not clear how this can be done globally on an operational basis (cf., discussion at the end in [8]). Thus, at the present time it appears that no satisfactory algorithm exists for the retrieval of LAI and FAPAR from satellite data. However, the state of art in canopy radiation modeling is significantly advanced, and with it our understanding of vegetation remote sensing [9]. Therefore, a physically based algorithm that is sufficiently simple and yet accurate would be highly desirable in the EOS era. This paper describes such an algorithm for the estimation of LAI and FAPAR from atmospherically corrected Normalized Difference Vegetation Index (NDVI) observations.

II. Theoretical Basis

There are many examples in published literature of NDVI–LAI and NDVI–FAPAR relations, either based on coincident measurements or model estimates (reviewed in [9]). While the general body of empirical evidence is convincing, a theoretical basis for the existence of these relations has been published only recently in this journal [10]. It was reported that most spectral vegetation indices can be generalized to show a derivative of surface reflectance with respect to wavelength. This derivative is a function of the optical properties of leaves and soil particles. In the case of optically dense vegetation, the spectral derivative, and thus the indices, are indicative of the abundance and activity of the absorbers in the leaves. Therefore, the widely used broad-band red/near-infrared vegetation indices, such as NDVI, are a measure of chlorophyll abundance and energy absorption.

The derivation presented in Myneni *et al.* [10] is generic, for it includes all published spectral vegetation indices, and the

Manuscript received November 21, 1995; revised January 27, 1997. This work was supported by grants from the Office of Mission to Planet Earth of NASA (Terrestrial Ecology Program, and MODIS-MISR Science Team Member Funds).

R. B. Myneni is with the Department of Geography, Boston University, Boston, MA 02215 USA (e-mail: rmyneni@crsa.bu.edu).

R. R. Nemani and S. W. Running are with the School of Forestry, University of Montana, Missoula, MT 59812 USA.

Publisher Item Identifier S 0196-2892(97)05517-4.

theoretical basis of NDVI–LAI and NDVI–FAPAR relations is not readily evident. Therefore, a simple summary is presented here, to establish a theoretical basis for the LAI/FAPAR algorithm to be discussed later.

Vegetation indices typically capture the absorption contrast across the 0.65–0.85-μm wavelength interval through combinations of broad-band red and near-infrared reflectance. The most widely used index in the processing of satellite data is the Normalized Difference Vegetation Index (NDVI) defined as $[(\rho_N - \rho_R)/(\rho_N + \rho_R)]$, where ρ_N and ρ_R are spectral bidirectional reflectance factors (ratio of the radiance of a target surface to the radiance of a conservative, lambertian surface) at near-infrared and red wavelengths, respectively. NDVI can be shown to be related to the derivative of surface reflectance with respect to wavelength [10]. To do so, let $\mathrm{NDVI} = \Delta V$, $\rho_N = \rho(\lambda + \Delta\lambda)$ and $\rho_R = \rho(\lambda)$. Note that

$$\rho(\lambda+\Delta\lambda) - \rho(\lambda) = \frac{d\rho}{d\lambda}\,\Delta\lambda \;+\; \Theta[(\Delta\lambda)^2]$$
$$\rho(\lambda+\Delta\lambda) + \rho(\lambda) = \frac{2}{\Delta\lambda}\int_{\lambda}^{\lambda+\Delta\lambda} d\lambda'\rho(\lambda') + \Theta[(\Delta\lambda)^2].$$

Here $\Theta(\Delta\lambda^2)$ denotes error of order $\Delta\lambda^2$. In the limit $(\Delta\lambda \to 0)$

$$\frac{dV}{d\lambda} = \frac{d\rho}{d\lambda}\,k$$

where $k = [1/2\rho(\lambda)]$. If one can now show that this spectral derivative is related to LAI and FAPAR, the theoretical basis of the relation established.

The spectral derivative can be written as

$$\frac{d\rho}{d\lambda} \approx \frac{\partial F}{\partial \rho_S}\frac{\partial Q}{\partial \omega_S}\frac{d\omega_S}{d\lambda} + \frac{\partial F}{\partial \omega_L}\frac{\partial P}{\partial \kappa}\frac{d\kappa}{d\lambda}. \tag{1}$$

In the above, ρ_S is soil reflectance, ω_S is soil particulate single scattering albedo, ω_L is leaf albedo and κ is the transmittance of a hypothetical unit layer of leaf interior. The functions F, Q, and P describe radiative transfer in a canopy of leaves layered above a soil surface, a semi-infinite medium of soil particles and the interior of a leaf modeled as a pile of transparent plates, respectively. The governing equations of transfer are linear integro-differential equations [9]. The solutions can be expressed formally as a sum of exponential functions, that is, the photon count decays exponentially through successive absorption and scattering events in the media. The partial derivatives ($\partial F/\partial\rho_S$, $\partial F/\partial\omega_L$, $\partial Q/\partial\omega_S$, and $\partial P/\partial\kappa$) are, therefore, exponential functions—smooth and smaller in magnitude than the total derivatives ($d\omega_S/d\lambda$ and $d\kappa/d\lambda$). In particular, $|(\partial F/\partial\rho_S)(\partial Q/\partial\omega_S)| \ll |d\omega_S/d\lambda|$ and $|(\partial F/\partial\omega_L)(\partial P/\partial\kappa)| \ll |d\kappa/d\lambda|$. Hence

$$\frac{d\rho}{d\lambda} \propto \frac{d\omega_S}{d\lambda} + \frac{d\kappa}{d\lambda}. \tag{2}$$

This conclusion is also confirmed empirically [10].

To derive an explicit analytical result connecting the surface reflectance to either canopy leaf area index or absorbed radiation, we consider the case of an optically dense canopy of lambertian, horizontal leaves. Canopy reflectance in this case is also lambertian. The canopy reflection function F can be expressed analytically and the partial derivative $\partial F/\partial\omega_L$ can therefore be evaluated

$$\begin{aligned}\frac{\partial F}{\partial \omega_L} &= Ł\left[\frac{1}{B}\,\Phi^-(\rho_S, X) - \frac{A}{B}\,\Phi^+(1, V)\right] \\ &= Ł\left\{\frac{\partial F}{\partial \omega_L}\right\}\end{aligned} \tag{3}$$

$$\begin{aligned}\Phi^{\pm}(x, y) = \frac{\partial W}{\partial \omega_L}\Big(Wxe_1 + \frac{x}{Ł}e_2 \pm ye_1\Big) \\ + \frac{1}{Ł}\frac{\partial y}{\partial \omega_L}[\exp(\pm p) - \exp(\mp p)]\end{aligned} \tag{4}$$

where $e_1 = \exp(p) - \exp(-p)$, $e_2 = \exp(p) + \exp(-p)$, $p = WŁ$, ρ_S is soil hemispherical reflectance, and Ł is leaf area index (W, X, and V are defined in den Dulk [12]). The derivative $d\kappa/d\lambda$ is, with $\kappa(\alpha) = (1-\alpha)\exp(-\alpha) + \alpha^2\mathrm{E}_1(\alpha)$ [11],

$$\begin{aligned}\frac{d\kappa}{d\lambda} &= \sum_{i=1}^{N} \wp_i\left\{\frac{d\tilde{a}_i}{d\lambda}[\exp(-\alpha_i)(\alpha_i - 2)\right. \\ &\qquad \left. + 2\alpha_i\mathrm{E}_1(\alpha_i)] - \tilde{a}_i\exp(-\alpha_i)\right\} \\ &= \sum_{i=1}^{N} \wp_i\Psi(\alpha_i)\end{aligned} \tag{5}$$

where $\alpha_i = \wp_i\tilde{a}_i$. Here $\mathrm{E}_1(\alpha)$ is exponential integral of order one and, α is the absorption coefficient given by the product of absorber concentration per unit leaf area $\wp$ and absorber specific absorption coefficient $\tilde{a}$. Since, N species may be active at wavelength λ, $\alpha(\lambda) = \sum_i^N \wp_i\tilde{a}_i(\lambda)$. In view of (3) and (5), the spectral derivative for the case of an optically dense canopy of lambertian, horizontal leaves can be written as

$$\frac{d\rho}{d\lambda} \equiv \frac{\partial P}{\partial \kappa}\left\{\frac{\partial F}{\partial \omega_L}\right\}\sum_{i=1}^{N} Ł_i\wp_i\Psi(\alpha_i). \tag{6}$$

Here $Ł_i$ is the total leaf area per unit ground area, over which the ith-absorber species is distributed. Consequently, $Ł_i\wp_i$ denotes the concentration of the ith-absorber species per unit ground area. Therefore

$$\frac{d\rho}{d\lambda} \propto \sum_{i=1}^{N} Ł_i\wp_i \propto \sum_{i=1}^{N} Ł_i\wp_i\tilde{a}_i \tag{7}$$

that is, the spectral derivative is indicative of the abundance and activity of the various absorbers pertaining to radiation absorption. If only one major absorber species, such as chlorophyll, is of interest, as it is in the case of vegetation remote sensing and if this species is uniformly distributed over the entire leaf area, then $Ł_i\wp_i \equiv Ł$, where Ł is the green leaf area index. And, $\tilde{a}_i \equiv \tilde{a}$, the chlorophyll absorption coefficient. Thus,

$$\frac{d\rho}{d\lambda} \propto Ł \propto Ł\tilde{a} \tag{8}$$

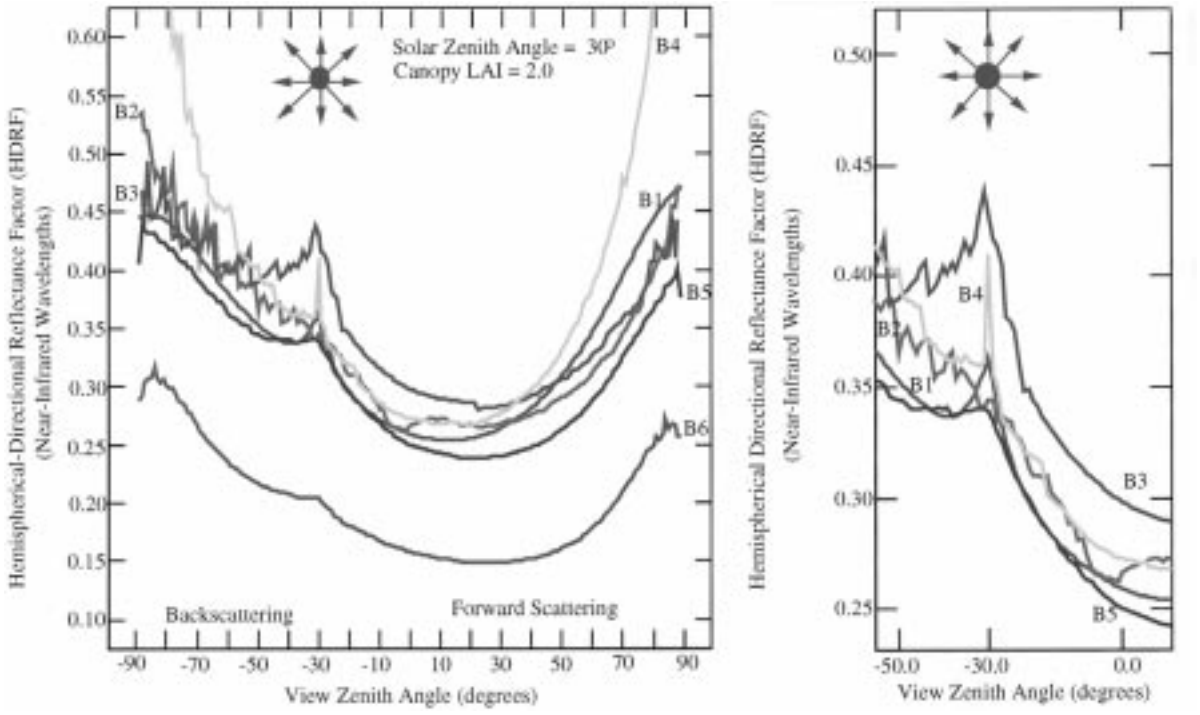

(a) (b)

Fig. 1. Hemispherical directional reflectance factors of the six land covers (Table I) at 30° sun zenith angle and combined under- and overstory leaf area index of 2. The notation B1, B2, B3, B4, B5, and B6 refers to cover types 1 through 6 defined in Table I: Grasses and Cereal Crops, Shrubs, Broadleaf Crops, Savannas, Broadleaf Forests, and Needle Forests. Panel (b) is a zoom-in of Panel (a) about the restro-solar view directions.

with $Ła$ denoting radiation absorbed by the chlorophyll in green leaves. This, then, is the theoretical basis for relating reflected radiations with canopy leaf area index, and the absorption of photosynthetically active radiation. It is important to note that the validity of the above theoretical development and conclusions is constrained by the assumptions made in obtaining (2) from (1), and (8) from (7). In practice, there are other influences on NDVI that confound a straightforward interpretation as to its meaning.

III. Canopy Structural Types of Global Vegetation

Although the cause and effect relation between NDVI and LAI/FAPAR can be established theoretically, its utility depends foremost on the sensitivity to canopy characteristics. For instance, if several canopies have a similar or a nearly similar NDVI–LAI relationship, information on such land covers is redundant for the estimation of LAI. As this is hardly the case, we must first stratify the global land covers into canopy structural types that have sufficiently different NDVI–LAI (or FAPAR) relations which warrant their use in order to satisfy the accuracy criterion. This implies that traditional land cover classifications based on botanical, ecological or functional metrics may be unsuitable for LAI/FAPAR estimations, because these classifications are not necessarily based on NDVI–LAI/FAPAR considerations [13]. Therefore, a land cover classification that is compatible with the LAI/FAPAR algorithm must be first developed.

Global land covers can be classified into six types depending on their canopy structure (Table I). The structural attributes of these land covers can be parameterized in terms of variables that the radiative transfer models admit. The six cover types are:

1) *Grasses and Cereal Crops:* Vertical and lateral homogeneity, vegetation ground cover of about 1.0, plant height generally less than a meter, erect leaf inclination, no woody material, minimal leaf clumping and intermediate soil brightness. The one-dimensional (1-D) radiative transfer model is invoked in this situation. Leaf clumping is implemented by modifying the projection areas with a clumping factor generally less than one.
2) *Shrubs:* Lateral heterogeneity, low (0.2) to intermediate (0.6) vegetation ground cover, small leaves, woody material and bright backgrounds. The full three-dimensional (3-D) model is invoked. Hot spot, i.e., enhanced brightness about the retro-solar direction due to absence of shadows [19], is modeled by shadows cast on the ground (no mutual shadowing as ground cover is low). This land cover is typical of semi-arid regions with extreme hot or cold (Tundra/Taiga) temperature regimes and poor soils.
3) *Broadleaf Crops:* Lateral heterogeneity, large variations in vegetation ground cover from crop planting to maturity (0.1 to 1.0), regular leaf spatial dispersion, photosynthetically active, i.e., green, stems and dark soil backgrounds. The regular dispersion of leaves (i.e., the positive binomial model) leads to a clumping factor that is generally greater than one. The green stems are modeled as erect reflecting protrusions with zero transmittance.
4) *Savanna:* Two distinct vertical layers, understory of grass, low ground cover of overstory trees ($\approx$0.2),

TABLE I
CANOPY STRUCTURAL ATTRIBUTES OF GLOBAL LAND COVERS FROM THE VIEWPOINT OF RADIATIVE TRANSFER MODELING

	Grasses / Cereal Crops	Shrubs	Broadleaf Crops	Savannas	Broadleaf Forests	Needle Forests
Horizontal Heterogeneity (Ground Cover)	No gc = 100%	Yes gc: 10-60%	Variable gc: 10-100%	Yes gc < 20%	Yes gc > 70%	Yes gc > 70%
Vertical Heterogeneity (Leaf Optics & LAD)	No	No	No	Yes	Yes	Yes
Stems/Trunks	No	No	Green Stems	Yes	Yes	Yes
Understory	No	No	No	Grasses	Yes	Yes
Foliage Dispersion	Minimal Clumping	Random	Regular	Minimal Clumping	Clumped	Severe Clumping
Crown Shadowing	No	Not Mutual	No	No	Yes Mutual	Yes Mutual
Background Brightness	Medium	Bright	Dark	Medium	Dark	Dark

TABLE II
COMPARISON OF THE LAND COVER CLASSIFICATION BASED ON RADIATIVE TRANSFER WITH THAT OF LOVELAND *et al.* [13]. NUMBERS IN PARENTHESIS ARE PERCENT OF THE TOTAL PIXELS IN EACH CLASS. SAVANNA BIOME IS NOT INCLUDED. BARREN PIXELS ARE SHOWN. THIS CLASSIFICATION IS FOR THE U.S. AT 1-km RESOLUTION

Running et al., 1994 & Loveland et al., 1991	Radiative Transfer Based Land Cover Classification				
	Grasses Cereal Crops	Shrubs	Broadleaf Crops	Broadleaf Forests	Needle Forests
Grasses/Cereal Crops	392 (63)	67 (11)	76 (12)	7	80 (13)
Shrubs	120 (21)	435 (77)	2	0	8
Broadleaf Crops	50 (13)	0	168 (44)	74 (19)	88 (23)
Broadleaf Forests	1	0	12	376 (73)	126 (24)
Needle Forests	41 (5)	0	6	148 (17)	676 (77)

canopy optics and structure are therefore vertically heterogeneous. The full 3-D method is required. The interaction coefficients have a strong vertical dependency. Savannas in the tropical and sub-tropical regions are characterized as mixtures of warm grasses and broadleaf trees. In the cooler regimes of the higher latitudes, they are described as mixtures of cool grass and needle trees.

5) *Broadleaf Forests:* Vertical and lateral heterogeneity, high ground cover, green understory, mutual shadowing by crowns, foliage clumping, trunks, and branches are included so that the canopy structure and optical properties differ spatially. Mutual shadowing by crowns is handled by modifying the hot spot formulation (next section). Therefore, stand density and crown size define this gap parameter. The branches are randomly oriented but tree trunks are modeled as erect structures. Both trunk and branch reflectance are specified from measurements.
6) *Needle Forests:* Needle clumping on shoots, severe shoot clumping in whorls, dark vertical trunks, sparse green understory, and crown mutual shadowing. This is the most complex case, invoking the full 3-D method with all its options. A typical shoot is modeled to handle needle clumping on the shoots. The shoots are then assumed to be clumped in the crown space. Mutual shadowing by crowns is handled by modifying the hot spot formulation. The branches are randomly oriented but the dark tree trunks are modeled as erect structures. Both trunk and branch reflectance are specified from measurements.

IV. RADIATIVE TRANSFER MODELING OF VEGETATION CLASSES

A radiative transfer model capable of simulating radiation scattering and absorption in the six structural classes defined

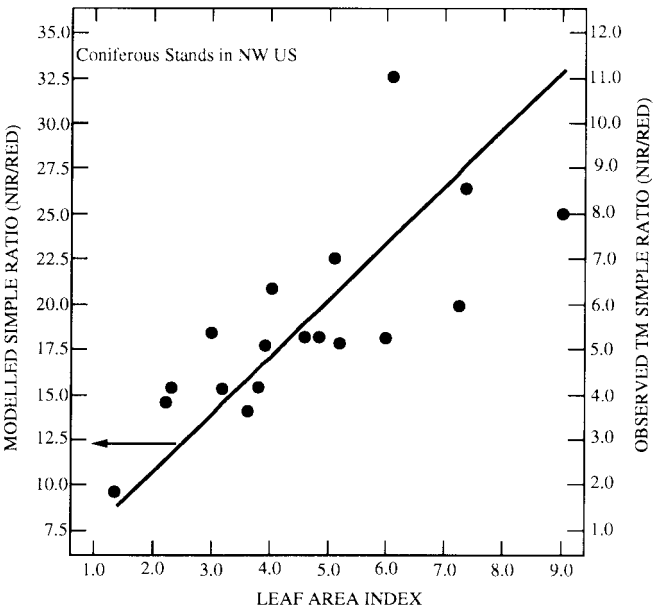

Fig. 2. Comparision between observed LANDSAT Thematic Mapper and radiative model simulated Simple Ratios (near-infrared to red reflectances) for various coniferous stands in the northwestern United States (Oregon, Montana, and California). The straight line is a linear fit to the simulated relationship between Simple Ratio and projected leaf area index. The magnitudes of the simulated and observed Simple Ratios are directly comparable although the latter have not been completely corrected for atmospheric effects, which in this instance can be clearly seen to have resulted in an offset of the observed Simple Ratios over the entire range of LAI values.

above is central to implementing the land cover classification and in estimating LAI/FAPAR from reflectance measurements. In this section, our published radiation modeling efforts are summarized and recent modeling activities are described.

Our initial efforts were concentrated on horizontally homogeneous, i.e., 1-D, canopies with the objective of simulating radiation interactions in broad leaf crops and grasslands. Considerable attention was paid to the derivation of appropriate scattering phase functions and their analytical solutions. The governing transport equations were numerically evaluated by the modified discrete ordinates method. The methods were benchmarked by comparing model results to published solutions [14]. The model results were compared to field measurements of soybean and maize reflectance measurements for trends and accuracy [15]. A finite element method was incorporated into this 1-D model to obtain fast and accurate numerical solutions [16]. The model was modified to include multiple vertical layers in order to simulate grassland reflectance [17] where the understory in unburned sites was litter from previous years. The model was also compared to a semi-analytical method and found to be four-digit accurate in most situations [18]. The model was numerically inverted with considerable success [19] and validated by Privette [20] with atmospherically corrected AVHRR data over the First International Field Experiment (FIFE) sites in a grassland prairie. The 1-D model was coupled to an atmospheric radiation model to simulate top of the atmosphere and canopy surface bidirectional reflectance distributions [21].

A formulation of the 3-D, i.e., horizontally and vertically heterogeneous, radiative transfer equation, the constituent interaction coefficients and its numerical solution were first reported in [22]. The method was partially validated with PAR transmission measurements in a cottonwood stand [23]. Its application to optical remote sensing of vegetation was illustrated and results on model comparison with reflectance measurements from a hardwood forest were presented [24]. The 3-D method was also validated extensively against shrublands reflectance measurements from a shrubland in the African Sahel [25] and found to reproduce the nonlinear canopy-soil interaction in sparse canopies well. The 3-D model was also used as a boundary condition in an atmospheric radiative transfer problem to study the adjacency effect [26]. The model has been used to benchmark several other methods and results on model intercomparisons with the discrete ordinate model as a reference were presented in [9].

Recent Model Developments: Leaf clumping was included in the formulation of the extinction and the differential scattering coefficients. The concept of particle distribution functions from statistical mechanics was utilized to derive analytical expression for leaf clumping [27]. A simplified model of leaf clumping based on this theory is now included in our model to simulate clumped, random and regular leaf dispersions in space. Vertical tree trunks and randomly oriented branches are also included in the current version of our model. Radiation interaction coefficients for the ensemble of leaves and trunks/branches are derived as linear mixtures with weighting proportional to their areal fractions. The absence of light transmission in trunks and branches imbues an asymmetry critical to the simulation of surface bidirectional reflectance in forest canopies. The hot spot model of Verstraete *et al.* [28] has been implemented in our radiative transfer formulation. This model is perhaps the most realistic of existing models of the hot spot effect and is driven by average gap size between leaves in a canopy. In forest canopies, however, where tree crowns mutually shade one another, crown shadowing has been implemented as the driver of the hot spot effect as opposed to gaps between leaves. The method of calculating mutual shadowing is based on the work of Li and Strahler [29], and its assimilation into the hot-spot model of Verstraete *et al.* [28] is rather ad hoc at the present time (i.e., the gap radius is derived iteratively from the proportions of illuminated and viewed crown and background). The resulting reflectance distributions show deepening of the bowl shape due to mutual shadowing, and are generally in good agreement with published results of Li and Strahler [29, Figs. 7–11]. Finally, in the case of needle canopies, geometric models of needle clumping on shoots and shoot clumping in whorls are implemented according to a formulation developed by Oker-Blom *et al.* [30]. With these developments, the model is seen to be reasonably well capable of simulating radiation scattering and absorption in the six land cover types identified earlier, i.e. grasses/cereal crops, shrubs, broadleaf crops, savannas, broadleaf, and needle forests. The model is currently being validated with data from a filed experiment in the Canadian boreal forests (BOREAS) and is being used extensively by the Moderate Resolution Imaging Spectro-Radiometer (MODIS)

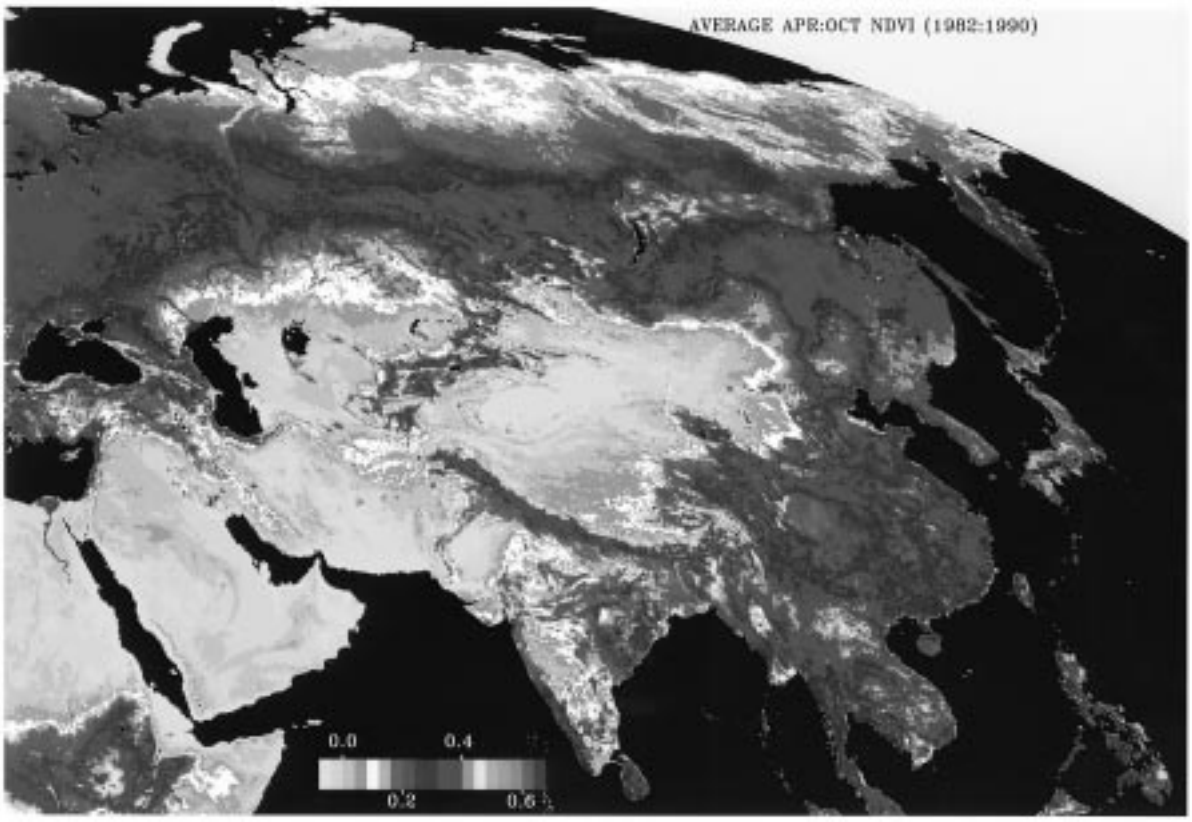

Fig. 3. Growing season average NDVI of Asia derived from the Advanced Very High Resolution Radiometer (AVHRR) Pathfinder data set [32]. Monthly NDVI was calculated as the average of three ten-day composites. The monthly values were further averaged over the nine-year period of record before Mount Pinotubo eruption (1982–1990) to obtain long-term average monthly NDVI values. Pixels with growing season average NDVI less than 0.04 were defined as nonvegetated areas and those greater than 0.08 as vegetated areas. Pixels with intermediate values were assigned to either of the two classes based on the distribution of the inverse of the coefficient of variation, which exhibits bimodality.

and Multi-angle Imaging Spectro-Radiometer (MISR) EOS-AM instrument science teams.

Example Simulations: The hemispherical directional reflectance factors (HDRF's), defined as the ratio of radiance of a vegetated surface to the radiance of a reference (conservative and Lambertian) surface under identical conditions of illumination (direct sunlight and diffuse skylight) and viewing, of the six land covers defined earlier were simulated in an effort to determine how the canopy structures affect the angular distribution of radiation emerging from these media. In all cases, canopy leaf area index (over- and understory) was 2.0, solar zenith angle was 30°, and the fraction of direct in total incident radiation was 0.8. The leaf and stem/trunk optical properties are given in Table III(b). The soil reflectance in the medium brightness class (Table III(c)) was used to parameterize the lower boundary condition. The fraction of stem, trunk, and branch area indices was varied from 10% (broadleaf crops) to 15% (forests) of the plant leaf area index. Canopy height was varied depending on the canopy type (0.8–1.2 m in land covers 1, 2, and 3, 10 m in land covers 4, 5, and 6). The tree crown dimensions were also varied (8×4 m in cover type 5 and 7×2 in cover type 6), to approximate wide and narrow crowns characteristic of broadleaf and needle canopies. Understory leaf area index was set to 0.5 in cover types 5 and 6. Calculations were performed at both red and near-infrared wavelengths. The results for the near-infrared waveband are shown in Fig. 1(a) and (b), to document the ability of the model to handle strong multiple scattering typical of vegetated surfaces at this waveband.

The angular distribution of HDRF's in the principal plane (i.e., the plane of the sun) shows the typical bowl shape, with backscattering generally greater than forward scattering, and a hot spot about the retro-solar direction. The simulation of cover type 1 invokes the 1-D turbid medium approximation of the plant canopy, and shows the characteristic HDRF distribution of vegetation canopies. The inclusion of vertical stems with reflectance similar to leaves and zero transmittance (broadleaf crops) has the effect of increasing the optical depth of the medium, i.e., overall reflectance increases because of increased multiple scattering. The hot spot is also broadened, as leaves of broadleaf crops are generally bigger than the thin elongated leaves in grasses and cereal crops. When a sparse overstory of trees (ground cover less than 20%) is introduced above the grass understory (savanna), the HDRF's at oblique views increase greatly because of long pathlengths through the under- and overstory canopy media. The hot spot in this instance is considerably narrow perhaps because the thin elongated leaves of the understory have smaller gap radii as in the case of grasses, but the height of the canopy now includes the overstory, an artifact that needs to be addressed. The effect of horizontally aggregating leaf area to reduce ground cover from 100% (grasses) to 50% (shrubs) is increased backscattering, decreased forward scattering and decreased variation around the retro-solar direction—effects that are primarily due to

TABLE III

(a) RADIATIVE TRANSFER MODEL PARAMETERS—TYPICAL VALUES AND RANGE. GROUND COVER IN BIOMES 4, 5, AND 6 REFERS TO THE OVERSTORY. THE TWO LEAF NORMAL ORIENTATIONS IN THESE BIOMES REFER TO OVER- AND UNDERSTORY. LEAF AND SOIL OPTICAL PROPERTIES AT RED AND NEAR-INFRARED BANDS ARE GIVEN IN (b) AND (c). THE STEM AND BRANCH FRACTIONS REFER TO THE FRACTION OF CANOPY LAI. (b) MEAN AND STANDARD DEVIATION (IN PARENTHESIS) OF LEAF AND BARK OPTICAL PROPERTIES DERIVED BY CONVOLVING SINGLE-LEAF SPECTRA WITH AVHRR BAND RESPONSE FUNCTIONS. OVER 150 SINGLE-LEAF AND BARK SPECTRA FROM VARIOUS SOURCES WERE ANALYZED TO OBTAIN THESE VALUES. (c) MEAN AND STANDARD DEVIATION (IN PARENTHESIS) OF SOIL (BACKGROUND) REFLECTANCES ESTIMATED FROM AVHRR PATHFINDER DATA. FOR EACH BIOME TYPE, THE COMPONENT CHANNEL REFLECTANCES AT YEARLY MINIMUM NDVI WERE PLOTTED TO IDENTIFY THOSE PIXELS WITH MINIMUM VEGETATION (RED/NEAR-INFRARED REFLECTANCE LINEARLY RELATED). THE CLASSIFICATION OF DARK, MEDIUM, AND BRIGHT WAS BASED ON EXAMINING THE FREQUENCY DISTRIBUTION OF THE RED REFLECTANCE. THE THRESHOLDS FOR EACH BIOME TYPE ARE AS FOLLOWS: (a) GRASSES AND CEREAL CROPS—DARK IS <9%, MEDIUM IS 10–19%, BRIGHT IS >19%; (b) SHRUBS—DARK IS <19%, MEDIUM IS 20–29%, BRIGHT IS >29%; (c) BROADLEAF CROPS—DARK IS <6%, MEDIUM IS 7–9%, BRIGHT IS >9%; AND (D) SAVANNA—DARK IS <8%, MEDIUM IS 9–12%, BRIGHT IS >12%

Parameter	Grasses/ Cereal Crops	Shrubs	Broadleaf Crops	Savanna	Broadleaf Forests	Needle Forests
Plant LAI	0 to 7	0 to 7	0 to 7	0 to 7	0 to 7	0 to 7
Ground Cover	1.0	0.2 to 0.6	0.1 to 1.0	0.2 to 0.4	> 0.8	> 0.7
Understory LAI	-	-	-	0 to 5	0 to 2	0 to 2
Leaf Normal Orientation	erectophile	uniform	uniform	uniform/ erectophile	uniform/ planophile	uniform/ planophile
Stems./Trunks & Branches	-	5%	10%	10%	15-20%	15-20%
Leaf Size (m)	0.05	0.05	0.10	-	-	-
Crown Size (m)	-	-	-	4 X 2 8 X 4	6 X 4 12 X 8	4 X 2 8 X 4
Solar Zenith Angle (deg)	10-60	10-60	10-60	10-60	10-60	10-60

(a)

BIOME	BAND 1 (RED)		BAND 2 (NIR)	
	Reflectance (%)	Transmittance (%)	Reflectance (%)	Transmittance (%)
GRASSES	11.64 (2.15)	11.24 (2.14)	42.71 (3.25)	47.90 (5.04)
SHRUBS	17.16 (7.84)	8.7 (7.25)	50.0 (8.86)	37.16 (8.55)
BROADLEAF CROPS	9.23 (1.12)	8.1 (1.8)	44.72 (4.23)	46.63 (3.92)
BROADLEAF FORESTS	7.90 (0.62)	7.3 (2.4)	43.09 (3.17)	42.96 (4.79)
(Bark)	26.17		65.35	
NEEDLE FORESTS	6.92 (2.78)	4.28 (3.58)	47.54 (6.40)	38.59 (7.77)
(Bark)	3.79		10.02	

(b)

BIOME	BAND 1 (RED) REFLECTANCE (%)			BAND 2 (NIR) REFLECTANCE (%)		
	Dark	Medium	Bright	Dark	Medium	Bright
GRASSES	6.5 (1.3)	11.2 (2.0)	23.3 (9.7)	7.9 (1.5)	13.2 (2.3)	26.9 (11.0)
SHRUBS	13.2 (3.0)	22.7 (2.3)	47.7 (10.7)	13.4 (4.0)	22.4 (3.0)	55.8 (14.0)
BROADLEAF CROPS	4.9 (1.0)	7.8 (0.8)	13.6 (4.0)	6.1 (1.0)	9.3 (0.9)	15.8 (4.6)
SAVANNA	6.5 (1.4)	10.1 (1.0)	15.3 (2.5)	7.8 (1.5)	11.9 (1.1)	17.8 (2.8)

(c)

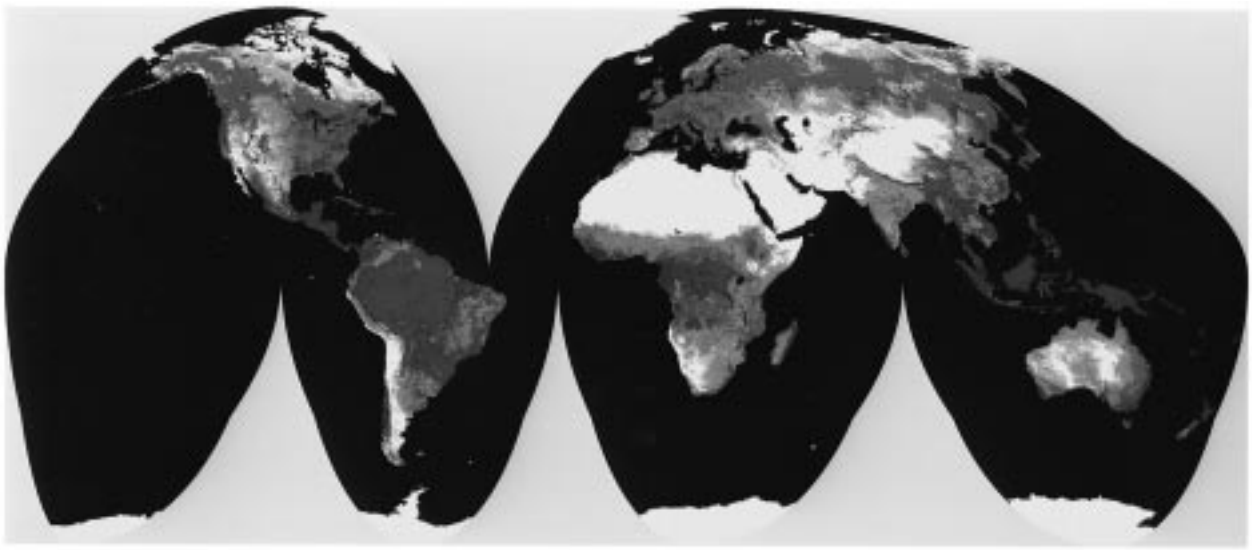

(a)

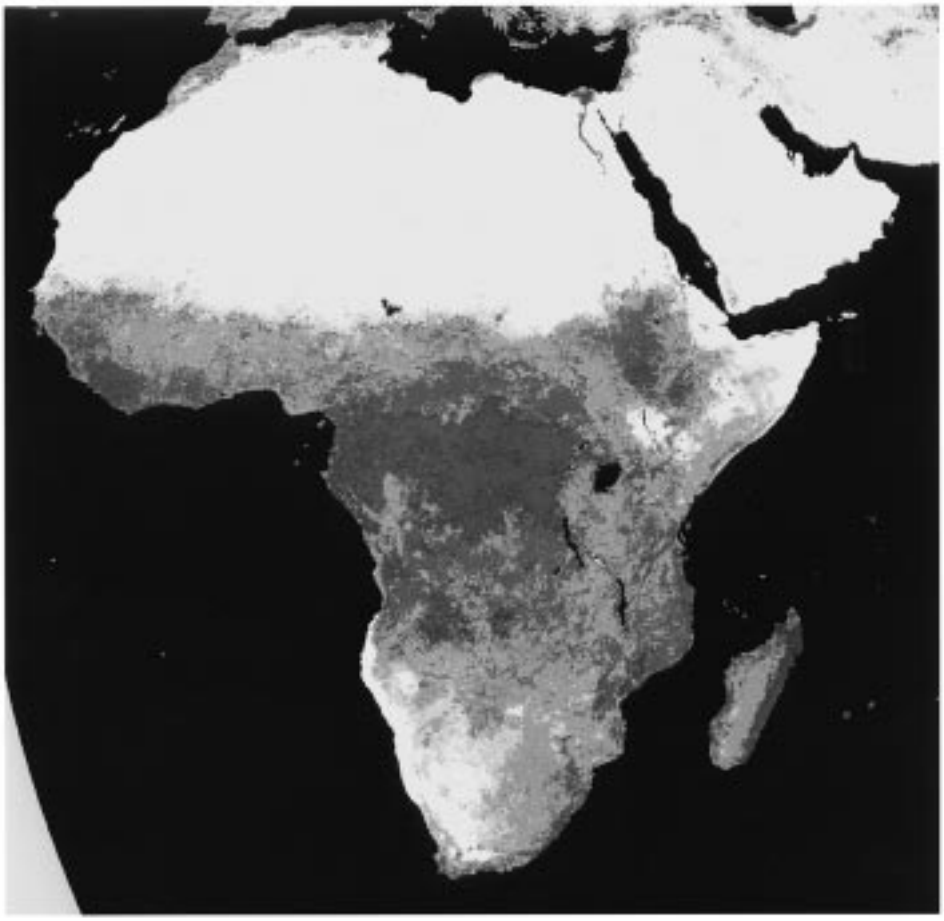

(b)

Fig. 4. Classification of global vegetation into land covers compatible with the radiative transfer models (Table I) used for the estimation of LAI and FAPAR: (a) global, (b) Africa. The color code is as follows: yellow is bare, green is grasses and cereal crops, brown is shrubs, dark green is broadleaf crops, red is savanna, blue is broadleaf forests, and magenta is needle forests.

increased interaction of the soil surface (note that the soil surface was modeled as a Lambertian diffuser in all cases). The inclusion of crown mutual shadowing (leaf forests) results in a deepening of the bowl shape and a broadening of the hot spot as it primarily increases the proportion of sunlit crowns along a given viewing direction. Finally, the inclusion of needle clumping and, trunks and branches darker than the needles, results in a decrease of the overall optical depth of the

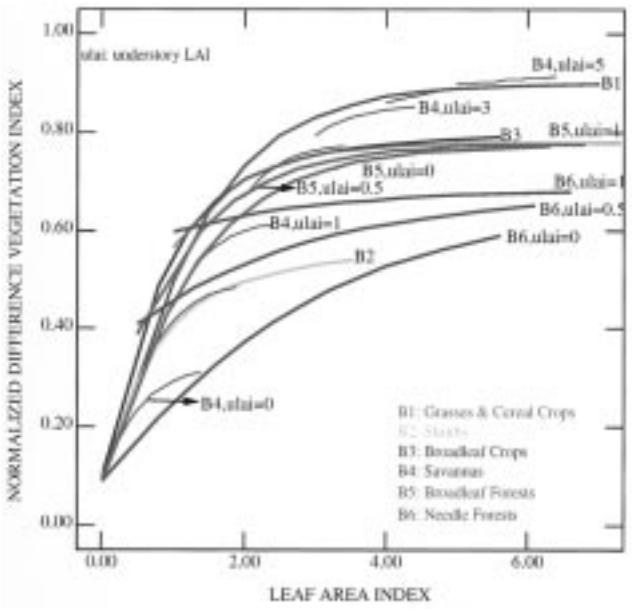

(a)

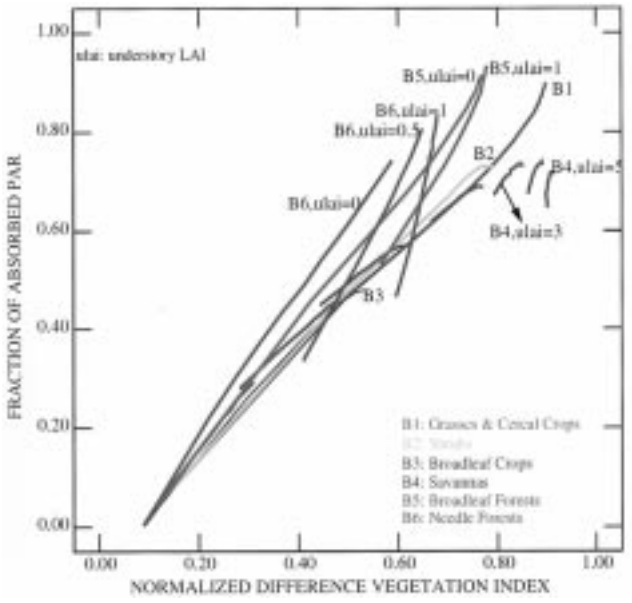

(b)

Fig. 5. Relationships between (a) NDVI–LAI and (b) NDVI–FAPAR for the six structural types of the landcover classification [Fig. 4(a)] simulated with the radiative transfer model in the base case scenario described in the text.

medium (needle forests), with HDRF's of considerably lower magnitude.

Validation: Leaf area index measurements of conifer forests in Northwestern United States described in [37], [38] were used to validate the improved radiative transfer model. LAI was estimated from allometric relations in 73 plots (0.1 acre) at 30 locations in Montana, 16 in Oregon, and 27 in California. The vegetation at these sites included many types of conifer stands (pines, spruces, juniper, etc). In order to reduce variance in LAI estimate at the Thematic Mapper (TM) scale, the plot level LAI estimates were aggregated to represent variations between vegetation zones controlled mainly by climate [37]. LAI estimates for the resulting vegetation zones (nine in Montana, six in Oregon, three in California) were used to compare with TM derived radiances. Landsat/Thematic Mapper data were acquired for the three regions during the summer of 1984. After locating the plots on imagery, data from near-infrared red (NIR) and Red channels were extracted and converted to radiances adjusted for terrain and partial atmospheric effects [38]. Simple Ratio (NIR/Red) for each of the 73 plots was calculated and then aggregated to represent the vegetation zones similar to LAI estimates. Red and NIR reflectances were simulated using the 3-D radiative transfer model recently modified for needle canopies as described above. A dark soil background and 75% ground cover were assumed in all the simulations. By changing tree LAI from 1 to 6 (canopy LAI from 0.75 to 4.5), Red and NIR reflectances were simulated to evaluate the Simple Ratio (SR). A highly significant linear relationship was found between canopy LAI and SR (SR $= 3.16 \times$ LAI $+ 4.4$, $r^2 = 0.9$). The relations between LAI and observed/simulated Simple Ratios are shown in Fig. 2. The modeled relation is very similar to that observed, thus indicating the ability of the model to reproduce radiative interactions in conifer stands in both these wavebands. However, the modeled and observed magnitudes of the Simple Ratio are not comparable, mostly due of atmospheric effects. The primary difference between the two seems to be a difference in offset, rather than the slope. Further validation of the model with data from boreal forests is currently underway.

V. Derivation of Vegetation Structural Types

The derivation of the above six canopy structural types from AVHRR Pathfinder data (8-km resolution) is presented here. Note that the six cover types defined above can also be obtained from traditional land cover classifications [13]. Nonvegetated areas (permanent snow, exposed soils, deserts, etc.) are first identified. Long-term monthly and yearly NDVI averages and standard deviations are examined to separate vegetated areas from nonvegetated areas. An example of the feasibility of this logic is shown in Fig. 3, where the April to September average NDVI of Asia is shown. The seasonally averaged NDVI value less than a threshold (0.04 NDVI in the case of AVHRR Pathfinder NDVI data) is the first metric used to identify bare areas. Similary, vegetated areas are identified by seasonally averaged NDVI values greater than a threshold (0.08 NDVI). The distribution of the coeffcient of variation (specifically, its inverse) of the remaining pixels is then examined for bi-modality and a threshold is selected to classify these pixels. While it is easier to identify areas that are definitely bare and those that are definitely vegetated, an element of subjectivity always remains in the classification of the intermediate pixels.

Vegetated areas are then divided into tropical, temperate, and boreal zones depending upon the duration of the freezing period. Within each of these zones, forests are first separated from nonforests based on the magnitude of NDVI at maximum surface temperature. The forested areas in the temperate and boreal zones can be further separated into leaf and needle forests by the magnitude of near-infrared

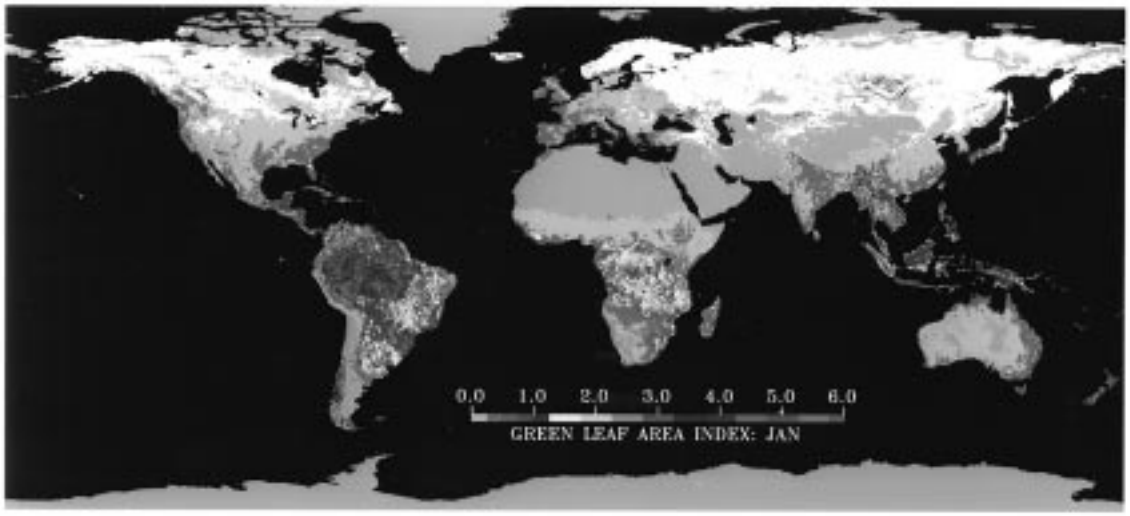

(a)

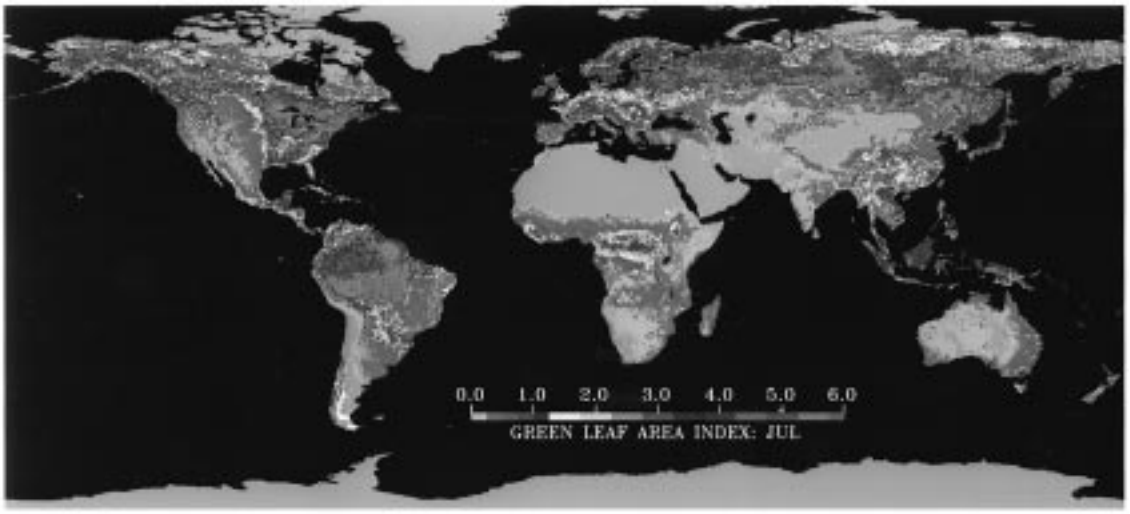

(b)

Fig. 6. Global leaf area index estimated with the NDVI–LAI relationships derived from the radiative transfer model and applied to the Advanced Very High Resolution Radiometer (AVHRR) Pathfinder NDVI data set [32]. The land cover-specific relations were applied to the ten-day composite NDVI data and the resulting LAI values were averaged to obtain monthly LAI at the 8 × 8 km native resolution of the Pathfinder data, and then aggregated to a 0.25° × 0.25° linear lat–long projection. This was done for all years from 1982 to 1990. Panel (a) shows the color-coded image of LAI in January obtained by further averaging over the nine-year period of record. Similarly, panel (b) shows the global LAI distribution during the month of July. Areas colored white denote either missing data (terminator effect) or where the algorithm failed.

reflectance at maximum NDVI [cf., Fig. 1(a)]. The nonforested areas are classified into savanna, broadleaf crops, shrubs, and grasses/cereals depending on the magnitude of red reflectance at maximum NDVI. The thresholds used in these classification are subjective and are specific to the NDVI data set used for classification. This classification scheme was implemented on the monthly composite 8-km AVHRR Pathfinder data [32]. The resulting land cover distribution is shown in Fig. 4(a) and (b). The classification for the US was compared with the landcover classification of Loveland *et al.* [13] which utilized an extensive amount of ancilliary information (Table II). The results indicate that Biomes 2, 5, and 6 can be identified successfully about 75% of the time. The worst case was broadleaf crops, which was misclassified 40% of the time as forests.

The land cover classification presented here has the advantage of being simple, operational and compatible with the radiation model used to derive LAI/FAPAR algorithm. It can be easily extended to higher resolution 1-km AVHRR data when these become available. The main disadvantage of this implementation strategy is the validity of the thresholds. Incomplete and/or incorrect atmospheric correction can result in misclassification. The impact of such misclassification on the estimation of LAI and FAPAR needs to be investigated. In addition to thresholds, we are investigating the utility of seasonally integrated greenness and ratio of backward to forward scattering as potential metrics for classification. The latter is especially promising as Multi-angle Imaging Spectro-Radiometer (MISR) data will be available in the EOS era.

VI. LAI/FAPAR Algorithm

The relationship between a spectral vegetation index such as NDVI and surface parameters LAI and FAPAR has been

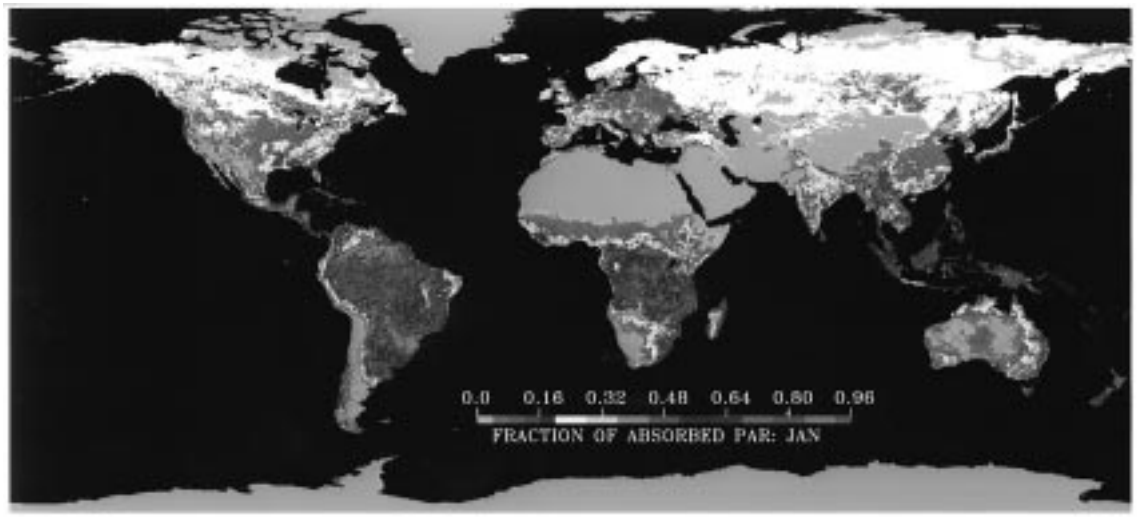

(a)

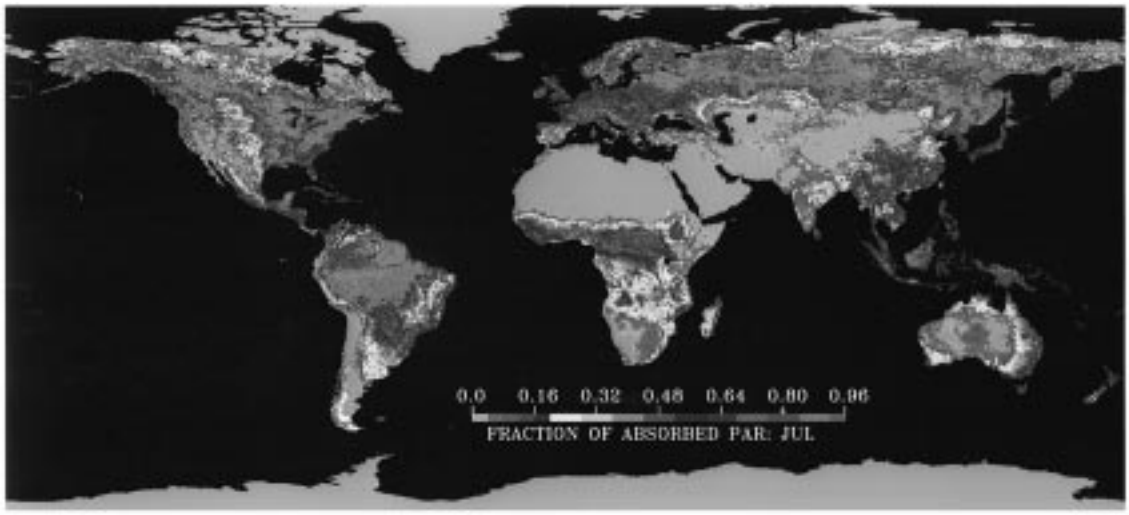

(b)

Fig. 7. Global fraction of absorbed PAR estimated with the NDVI–FAPAR relationships derived from the radiative transfer model and applied to the Advanced Very High Resolution Radiometer (AVHRR) Pathfinder NDVI data set [32]. The method of evaluating FAPAR is similar to that used for LAI estimation (Fig. 6).

extensively studied (reviewed in [10]). The theoretical basis of these relations was given earlier. We propose to utilize these relations for the estimation of LAI and FAPAR, after assessing their robustness with respect to variations in ancillary parameters of the surface and measurement geometry. Standard canopies of the six land covers described earlier were defined in terms of parameter values considered typical from a remote sensing point of view (Table III(a)–(c)). These canopies will be hereafter referred to as the base cases. The base case of each land cover consisted of 13 canopies of varying leaf area indices (0.1–7.0). In the case of savanna and forest land covers, a range of understory leaf area index was also considered (0.0–5.0). Spectral reflectance and absorbtance at red, near-infrared and PAR wavelength bands were calculated for all the 208 canopies of the six land covers with the radiative transfer discussed earlier. The resulting NDVI–LAI and NDVI–FAPAR relations are shown in Fig. 5(a) and (b).

The relationship between NDVI and LAI is nonlinear and exhibits considerable variation among the cover types. Not surprisingly, the relationships for vertically inhomogeneous land covers such as the savanna and forests are strongly dependent on the understory leaf area index [Fig. 5(a)]. There is practically no sensitivity in NDVI to overstory LAI in forest canopies with a dense understory. NDVI of leaf canopies such as grasses and crops always tends to be higher than forest canopies with similar LAI, because the tree trunks and branches in the latter tend to decrease near-infrared scattering, and therefore low NDVI values. The effect of leaf clumping can also be seen by comparing the NDVI values of needleleaf forest canopies with the broadleaf forest canopies at similar LAI values.

The NDVI–FAPAR relations are linear in most cases, with the exception of canopies with bright NDVI backgrounds (high understory LAI) [Fig. 5(b)]. These relationships are similar to those reported in the literature based on field data and model results [33]–[35]. However, the sensitivity of these relationships to problem parameters, especially sun and view

TABLE IV
CHANGES IN NDVI DUE TO VARIATIONS IN RADIATIVE TRANSFER MODEL PARAMETERS. NDVI CHANGES ARE RELATIVE TO THE BASE CASE NDVI. THE GROUND COVER IN THE BASE CASE OF THE SIX BIOMES IS 1.0, 0.5, 0.8, 0.2, 0.9, AND 0.8. THE SOLAR ZENITH ANGLE IS 30°. THESE CHANGES IN NDVI MUST BE SEEN AS TYPICAL CHANGES ONE COULD ENCOUNTER WHEN THE CANOPIES ARE GREEN AND EXHIBITING SEASONAL MAXIMUM NDVI

	Grasses/ Cereal Crops	Shrubs	Broadleaf Crops	Savanna	Broadleaf Forests	Needle Forests
Base Case	0.81	0.42	0.72	0.58	0.77	0.74
Ground Cover	-	-0.07 @ 0.4 0.07 @ 0.6	-0.17 @ 0.6 0.13 @ 1.0	-0.07 @ 0.1 0.12 @ 0.4	-0.01 @ 0.6 -	-0.03 @ 0.6 0.03 @ 1.0
Planophile	0.04	0.06	0.04	0.03	0.03	0.03
Uniform	0.01	-	-	-	-	-
Erectophile	-	-0.02	-0.02	-0.01	-0.01	-0.01
Gap Radius 10% change	-0.01	-0.01	-0.01	-0.04	-0.07	-0.08
Woody Material Fraction 10-40%	-	0.01 - 0.03	-	0.01 - 0.04	0.02 - 0.06	0.04 - 0.06
Bright Soil	-0.01	-	-0.04	-0.03	-0.01	-0.02
Medium Soil	-	0.04	-	-	-	-
Dark Soil	0.02	0.13	0.05	0.06	0.01	0.03
Sun Zenith Angle 15-60 deg	-0.01	-0.04	-0.07	-0.06	-0.01	-0.03

TABLE V
CHANGES IN LAI DUE TO CHANGES IN NDVI AS A RESULT OF RADIATIVE TRANSFER MODEL PARAMETER CHANGES. THE CORRESPONDING NDVI CHANGES ARE SHOWN IN A SIMILAR TABLE

	Grasses/ Cereal Crops	Shrubs	Broadleaf Crops	Savanna	Broadleaf Forests	Needle Forests
Base Case	3.34	1.12	2.60	1.84	3.86	5.45
Ground Cover	-	-0.50 @ 0.4 0.70 @ 0.6	-1.31 @ 0.6 1.45 @ 1.0	-0.43 @ 0.1 0.89 @ 0.4	-0.15 @ 0.6 -	-0.56 @ 0.6 0.53 @ 1.0
Planophile	0.38	0.53	0.40	0.17	0.39	0.56
Uniform	0.13	-	-	-	-	-
Erectophile	-	-0.16	-0.18	-0.06	-0.15	-0.16
Gap Radius 10% change	-0.05	-0.05	-0.04	-0.17	-0.12	-0.09
Woody Material Fraction 10-40%	-	0.07 - 0.14	-	0.08 - 0.19	0.13 - 0.24	0.16 - 0.31
Bright Soil	-0.12	-	-0.37	-0.21	-0.05	-0.40
Medium Soil	-	0.39	-	-	-	-
Dark Soil	0.19	1.51	0.48	0.46	0.03	0.64
Sun Zenith Angle 15-60 deg	-0.13	-0.31	-0.61	-0.36	-0.18	-0.54

geometry and background brightness, is the critical issue that determines the utility of these relations.

A sensitivity analysis was performed by changing the base case parameter values of each land cover, one at a time, to the end points of the parameter ranges typically encountered in practice. For instance, the leaf normal orientation of leaf forests in the base case simulation was assumed to be uniform [Table III(a)]. The sensitivity to leaf orientation in this land cover was investigated by changing the leaf normal orientation to planophile (mostly horizontal leaves) and repeating all the calculations that were performed in the base case simulation. Another set of calculations was performed with

erectophile leaf normal orientation (mostly erect leaves). In this fashion, the NDVI–LAI and NDVI–FAPAR relationships were repeatedly simulated for various scenarios to investigate the sensitivity to ground cover, understory LAI, leaf normal orientation, woody material fraction, leaf and crown sizes, soil reflectance, and solar zenith angle. The sensitivity analysis is similar to that described in greater detail in our previous papers [35], [36]. All the data were then regressed to obtain land cover specific NDVI–LAI and NDVI–FAPAR relations that were statistically significant. These together with the land cover classification were then used to estimate LAI and FAPAR—the results thus obtained are shown in Figs. 6 and 7. The algorithm is valid for view and sun zenith angles less than 60°. The LAI/FAPAR results depicted must be seen as proof-of-concept because the relations require NDVI evaluated from atmospherically corrected reflectances. Although the AVHRR pathfinder data was cloud screened, composited, and corrected for Rayleigh and ozone effects, more importantly it was not corrected for aerosol scattering and water vapor absorption. Therefore, the dynamic between the end points of these relations had to be matched by percentile with the observed range in the AVHRR Pathfinder NDVI data [7].

Table IV depicts the variations in nadir NDVI for typical changes in the radiative transfer model parameters and solar zenith angles. Since the NDVI–FAPAR relationship is (near) linear, the error in the estimation of FAPAR because of uncertainty in the problem parameters is of the same order of magnitude as that given in Table IV for NDVI. Large variations in NDVI and FAPAR (ca., 0.1) can occur if the ground cover is not precisely known. Similar errors occur for shrubs if the soil reflectance is incorrectly specified (Table IV). The NDVI–LAI relationship, however, is nonlinear; errors in LAI estimates due to NDVI variations (Table IV) are shown in Table V. It appears that in most cases uncertainty in the LAI estimate may be of the order of 0.5 LAI. These estimates are valid for canopies at seasonal maximum greenness. A similar analysis is required for the green-up and senescent phases. Whether or not this is within the tolerable range depends on the application for which such a LAI product is intended.

VII. Concluding Remarks

The estimation of surface parameters of interest in global climate and biogeochemistry models from satellite observations is a challenging task. Even when properly calibrated, cloud screened and atmospherically corrected data are available, the linkages between surface reflectance and canopy variables such as LAI and FAPAR are often not straightforward as noise due to measurement geometry and soil properties can be substantial. Nevertheless, the analysis presented here shows that a simple algorithm can be developed to estimate LAI and FAPAR from satellite data. The emphasis is of necessity on algorithmic simplicity and reasonable accuracy, for automated operational processing of satellite data even at 1-km spatial resolution and ten-day temporal frequency is tedious with present-day computers. Higher spatial and temporal resolutions are planned for the EOS era. The algorithms reported in this paper must therefore be viewed within a framework dominated largely by practical considerations and to a lesser extent by accuracy.

Acknowledgment

The authors gratefully acknowledge the support of NASA. Many individuals contributed their spectral data which were used to obtain the leaf and soil optical properties reported here, and the authors gratefully acknowledge their contribution (Dr. Asner, Dr. Clark, Dr. Hall, Dr. Hanan, Dr. Jacquemoud, Dr. Schimel, and Dr. Verstraete).

References

[1] P. J. Sellers and D. S. Schimel, "Remote sensing of the land biosphere and biogeochemistry in the EOS era: Science priorities, methods and implementation—EOS land biosphere and biogeochemical cycles panels," *Global and Planetary Change*, vol. 7, pp. 279–297, 1993.

[2] R. B. Myneni, S. O. Los, and G. Asrar, "Potential gross primary productivity of terrestrial vegetation from 1982–1990," *Geophys. Res. Lett.*, vol. 22, pp. 2617–2620, 1995.

[3] G. Asrar and D. J. Dokken, Eds., *EOS Reference Handbook.* Washington, DC: NASA, 1993.

[4] A. Ruimy, B. Saugier, and G. Dedieu, "Methodology for the estimation of net primary production from remotely sensed data," *J. Geophys. Res.*, vol. 99, pp. 5263–5283, 1994.

[5] P. J. Sellers, Y. Mintz, Y. C. Sud, and A. Dalcher, "A simple biosphere model (SiB) for use within general circulation models," *J. Atmos. Sci.*, vol. 43, pp. 505–531, 1986.

[6] S. O. Los, C. O. Justice, and C. J. Tucker, "A global 1 × 1 NDVI data set for climate studies derived from the GIMMS continental NDVI data," *Int. J. Remote Sens.*, vol. 15, pp. 3493–3518, 1994.

[7] P. J. Sellers, S. O. Los, C. J. Tucker, C. O. Justice, D. A. Dazlich, C. J. Collatz, and D. A. Randall, "A 1 × 1 NDVI data set for global climate studies. Part 2: The generation of global fields of terrestrial biophysical parameters from the NDVI," *Int. J. Remote Sens.*, vol. 15, pp. 3519–3545, 1994.

[8] J. C. Price, "Estimating leaf area index from satellite data," *IEEE Trans. Geosci. Remote Sensing*, vol. 31, pp. 727–734, 1993.

[9] R. B. Myneni, S. Maggion, J. Iaquinta, J. L. Privette, N. Gobron, B. Pinty, M. M. Verstraete, D. S. Kimes, and D. L. Williams, "Optical remote sensing of vegetation: Modeling, caveats and algorithms," *Remote Sens. Environ.*, vol. 51, pp. 169–188, 1995.

[10] R. B. Myneni, F. G. Hall, P. J. Sellers, and A. L. Marshak, "The interpretation of spectral vegetation indices," *IEEE Trans. Geosci. Remote Sensing*, vol. 33, pp. 481–486, 1995.

[11] S. Jacquemoud and F. Baret, "PROSPECT: A model of leaf optical properties spectra," *Remote Sens. Environ.*, vol. 34, pp. 75–91, 1990.

[12] J. A. den Dulk, "The interpretation of remote sensing, a feasibility study," Ph.D. thesis, The Agricultural Univ. Wageningen, The Netherlands, 1989, p. 145.

[13] T. R. Loveland, J. W. Merchant, D. O. Ohlen, and J. F. Brown, "Development of a land cover characteristic data base for the conterminous U.S.," *Photgramm. Eng. Remote Sens.*, vol. 57, pp. 1453–1463, 1991.

[14] R. B. Myneni, V. P. Gutschick, G. Asrar, and E. T. Kanemasu, "Photon transport in vegetation canopies with anisotropic scattering: Parts I through IV," *Agricult. Forest Meteorol.*, vol. 42, pp. 1–16, 17–40, 87–99, and 101–120, 1988.

[15] J. K. Shultis and R. B. Myneni, "Radiative transfer in vegetation canopies with anisotropic scattering," *J. Quant. Spectrosc. Radiat. Transf.*, vol. 39, pp. 115–129, 1988.

[16] R. B. Myneni, G. Asrar, and E. T. Kanemasu, "Finite element discrete ordinates method for radiative transfer in nonrotationally invariant scattering media: Application to the leaf canopy problem," *J. Quant. Spectrosc. Radiat. Transf.*, vol. 40, pp. 147–155, 1988.

[17] G. Asrar, R. B. Myneni, Y. Li, and E. T. Kanemasu, "Measuring and modeling spectral characteristics of a tallgrass prairie," *Remote Sens. Environ.*, vol. 27, pp. 143–155, 1989.

[18] B. D. Ganapol and R. B. Myneni, "The F_N method for the one-angle radiative transfer equation applied to plant canopies," *Remote Sens. Environ.*, vol. 39, pp. 61–74, 1992.

[19] J. L. Privette, R. B. Myneni, W. L. Emery, and C. J. Tucker, "Invertibility of a 1D discrete ordinates canopy reflectance model," *Remote Sens. Environ.*, vol. 48, pp. 89–105, 1994.

[20] J. L. Privette, "An efficient strategy for the inversion of bidirectional reflectance models with satellite remote sensing data," Ph.D. thesis, Univ. Colorado, Boulder, 1994.
[21] R. B. Myneni, I. Impens, and G. Asrar, "Simulation of space measurements of vegetation canopy bidirectional reflectance factors," *Remote Sens. Rev.*, vol. 7, pp. 19–41, 1993.
[22] R. B. Myneni, G. Asrar, and S. A. W. Gerstl, "Radiative transfer in three dimensional leaf canopies," *Trans. Theory Stat. Phys.*, vol. 19, pp. 205–250, 1990.
[23] R. B. Myneni, "Modeling radiative transfer and photosynthesis in three dimensional vegetation canopies," *Agric. Forest Meteorol.*, vol. 55, pp. 323–344, 1991.
[24] R. B. Myneni, G. Asrar, and F. G. Hall, "A three dimensional radiative transfer method for optical remote sensing of vegetated land surfaces," *Remote Sens. Environ.*, vol. 41, pp. 105–121, 1992.
[25] A. Begue and R. B. Myneni, "Relationships between NOAA-AVHRR vegetation indices and daily FAPAR established for sahelian vegetation canopies," *J. Geophys. Res.*, (submitted in Sept. 1995).
[26] R. B. Myneni and G. Asrar, "Radiative transfer in three dimensional atmosphere vegetation media," *J. Quant. Spectrosc. Radiat. Transf.*, vol. 49, pp. 585–598, 1993.
[27] ———, "Photon interaction cross sections for aggregations of finite dimensional leaves," *Remote Sens. Environ.*, vol. 37, pp. 219–224, 1991.
[28] M. M. Verstraete, B. Pinty, and R. E. Dickinson, "A physical model for predicting bidirectional reflectances over bare soils," *Remote Sens. Environ.*, vol. 27, pp. 273–288, 1989.
[29] X. Li and A. H. Strahler, "Geometric-optical bidirectional reflectance modeling of the discrete crown vegetation canopy: Effect of crown shape and mutual shadowing," *IEEE Trans. Geosci. Remote Sensing*, vol. 30, pp. 276–292, 1992.
[30] P. Oker-Blom, J. Lappi, and H. Smolander, "Radiation regime and photosynthesis of coniferous stands," in *Photon Vegetation Interactions*, R. B. Myneni and Ross, Eds. Berlin, Germany: Springer-Verlag, 1991, pp. 501–535.
[31] R. B. Myneni and D. L. Williams, "A radiative transfer model for remote sensing of boreal forests," *J. Geophys. Res.*, submitted for publication.
[32] M. E. James and S. N. V. Kalluri, "The Pathfinder AVHRR land data set: An improved coarse-resolution data set for terrestrial monitoring," *Int. J. Remote Sens.*, vol. 15, pp. 3347–3364, 1994.
[33] D. L. Peterson, M. A. Spanner, S. W. Running, and L. Band, "Relationship of Thematic Mapper Simulator data to leaf area index," *Remote Sens. Environ.*, vol. 22, pp. 323–341, 1987.
[34] G. Asrar, M. Fuchs, E. T. Kanemasu, and J. L. Hatfield, "Estimating absorbed photosynthetic radiation and leaf area index from spectral reflectance in wheat," *Agron. J.*, vol. 76, pp. 300–306, 1984.
[35] R. B. Myneni, G. Asrar, D. Tanré, and B. J. Choudhury, "Remote sensing of solar radiation absorbed and reflected by vegetated land surfaces," *IEEE Trans. Geosci. Remote Sensing*, vol. 30, pp. 302–314, 1992.
[36] R. B. Myneni and D. L. Williams, " On the relationship between FAPAR and NDVI," *Remote Sens. Environ.*, vol. 49, pp. 200–211, 1994.
[37] D. L. Peterson, and S. W. Running, "Applications in forest science and management," in *Theory and Applications of Optical Remote Sensing*, G. Asrar, Ed. New York: Wiley, 1989, pp. 429–473.
[38] M. A. Spanner, L. Pierce, D. L. Peterson, and S. W. Running, "Remote sensing of temperate conifer forest leaf area index: Influence of canopy closure, understory vegetation and background reflectance," *Int. J. Remote Sensing*, vol. 11, pp. 95–111, 1990.

Ranga B. Myneni received the Ph.D. degree in biology from the University of Antwerp, Antwerp, Belgium, in 1985.

Since then, he has worked at Kansas State University, Manhattan, the University of Göttingen, Germany, and NASA Goddard Space Flight Center, Greenbelt, MD. He is now on the faculty of the Department of Geography, Boston University, Boston, MA. His research interests are radiative transfer, remote sensing of vegetation, and climate-vegetation dynamics.

Dr. Myneni is a MODIS and MISR science team member.

Ramakrishna R. Nemani studied agronomy and meteorology in India, and received the B.S. degree from A.P. Agricultural University, Hyderabad, and the M.S. degree from Punjab Agricultural University, Ludhiana. He receievd the Ph.D. degree in forest ecology from the University of Montana, Missoula, in 1987.

He is a Research Associate Professor at the University of Montana. His current interests include extraction of biophysical information about land surfaces (leaf-area index, surface wetness, and land cover) from remote sensing observations, and ecosystem modeling at continental to global scales.

Dr. Nemani is an associate team member of the American Geophysical Union.

Steven W. Running was trained as a terrestrial ecologist and received the B.S. and M.S. degrees from Oregon State University, Corvallis, and the Ph.D. degree from Colorado State University, Fort Collins.

He has been at the University of Montana, Missoula, since 1979, and is now a Professor of forestry. His primary research interest is the development of global and regional ecology by integration of remote sensing with climatology and terrestrial ecology using computer simulation.

Dr. Running is a member of the Scientific Steering Committee for the Biospheric Aspects of the Hydrologic Cycle project of the International Geosphere–Biosphere Program. He is also a team member for the NASA Earth Observing System, Moderate Resolution Imaging Spectroradiometer (EOS/MODIS).